ACS EARTH AND SPACE CHEMISTRY

http://pubs.acs.org/journal/aesccq

Article

Preferably Plinian and Pumaceous: Implications of Microbial Activity in Modern Volcanic Deposits at Askja Volcano, Iceland, and Relevancy for Mars Exploration

Erika Rader, Anna Simpson, Elena Amador, Julia M. Fraser, Samuel Holtzen, Ashley Hanna, Morgan L. Cable, Thomas Cullen, Zach Duca, Diana Gentry, Gayathri Murukesan, Vincent Rennie, Adam H. Stevens, Scot Sutton, George Tan, David Cullen, Wolf Geppert, and Amanda Stockton*

Cite This: https://dx.doi.org/10.1021/acsearthspacechem.0c00015

Read Online

ACCESS | Metrics & More | Article Recommendations | Supporting Information

ABSTRACT: To search more efficiently for a record of past life on Mars, it is critical to know where to look and thus maximize the likelihood of success. Large-scale site selection for the Mars 2020 mission has been completed, but small (meter to 10 cm)-scale relationships of microenvironments will not be known until the rover reaches the surface. Over a 2 m transect at a modern volcanic deposit on the flank of Askja volcano in the barren highlands of Iceland, we compared two biological indicators (ATP activity and 16SrRNA amplicon sequence composition) to physical characteristics including bulk chemical composition, spectral signatures of mineralogy, and grain size. Using analytical instrumentation analogous to those available on Mars rovers, we were able to characterize the geological setting of the deposits and link physical parameters to microbial abundance and diversity. In general, methanogenesis, methanotrophy/methylotrophy, and nitrate reduction were the functional traits most associated with microbial community shift along the transect. Core microbiome members tended to be associated with nitrate reduction, and relative abundance of core microbes was strongly related to free water in the deposit. Community compositional shift of the rare microbiome was related to microenvironmental changes such as change in grain size, geochemistry, and age of deposit. These correlations lead us to suggest a sampling strategy that accounts for Martian geology, looking for undisturbed (not remobilized) explosive volcanic ash below pumice that could maximize diversity and abundance of different bioindicators. Our study also illustrates the importance of studying the variability across microenvironments in low biomass settings on earth.

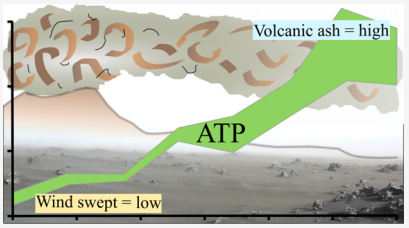

KEYWORDS: *astrobiology, volcanology, explosive, geochemistry, Mars, VNIR*

INTRODUCTION

Iceland as an Astrobiological Analogue. The highlands of Iceland have low bioabundance and extensive sandy volcanic deposits, similar to Mars.[1−5] The chemical and geologic diversity that develops in this environment is a good representation of the diversity in surfaces in which ancient lifeforms would have evolved, adapted, and been preserved. The cold, barren, and exposed landscape around the Askja volcano provides a volcanologically well-constrained event, which resulted in physically and chemically diverse environments in a very compact area, thus excluding effects from microclimates or spatial differences.

Askja Geological Background. The Askja volcano in Iceland lies over the hot spot-enhanced mid-ocean ridge that separates the North American Plate to the west and the European Plate to the east.[4] This lake-filled caldera-forming volcano has historically erupted everything from mafic effusive lava flows to silicic explosive pumice fall deposits.[6] Askja had a major catastrophic (Plinian) eruption in 1875, which rained down ash and pumice which blanketed the northeastern region of Iceland.[6] These deposits still remain today as unweathered, unaltered, unrounded, and unvegetated layers on top of the wind-blown sandy desert.

The targeted sampling location contained two primary components, an older aeolian sandy desert layer (sandur) common in the highlands of Iceland and a younger volcanic fall deposit from the 1875 eruption of the Askja volcano.[1] The older volcanoclastic layer of sediment composed of wind-blown clasts that covers >20,000 km^2 and is the result of harsh weather, high erosion rates, and abundant volcanic source materials.[1−5] This wind-blown mixture of regional volcanic products includes pyroclastics, eroded lava clasts, and dark-colored sand, all of which predate the 1875 eruption. The general chemical composition of the sandur is basaltic and made up mostly of glass particles; however, andesitic and rhyolitic are also blown in from the moraines of Vatnajökull over 30 km away.[1]

Received: January 14, 2020
Revised: July 20, 2020
Accepted: July 29, 2020
Published: July 29, 2020

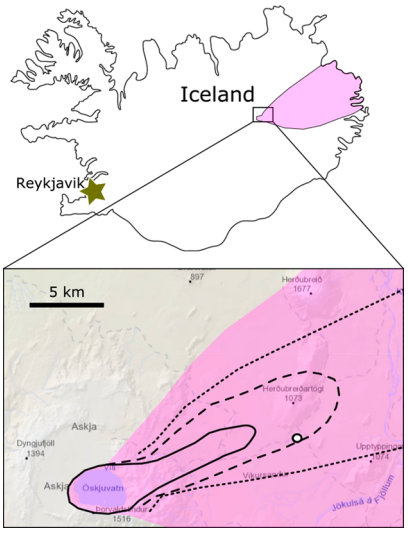

Figure 1. Map of the 0.1 cm-thick Layer C deposits of the 1875 Askja eruption in pink. The zoomed-in area shows 2.5, 5, and 10 cm-thick deposits (dotted, dashed, and solid lines, respectively) from Carey et al.[8] Sample location for this study is the small white circle.

On top of the sandur in this location, the 1875 eruption deposited two horizons of a deposit called the "C layer" on the 28th−29th of March.[6,7] The C layer is ash and pumice widespread across NE Iceland (see the pink outline in Figure 1) and the thickness decreases with the distance from the vent (Öskjuvatn) as indicated by isopach lines in the same figure[8] The grains in the C layer are high in SiO_2, well-sorted, and very angular.[9] They are made up of predominantly volcanic glass in the form of sharp pumice fragments.[10,11] The mineral content of the ash and pumice is ∼5% and is made up of plagioclase, pyroxene, iron oxides, and a mention of trace apatite.[11] The Askja ash characteristics are in sharp contrast to those of the sandur sediment, which experienced more collisions with other grains during transport and thus are smaller and more rounded.[1,12]

Plinian eruptions, like the one in 1875, are the most violent and explosive of the eruption classification system[13] and often result in widespread deposits of ash and/or pumice.[14] These mega eruptions can produce deposits with basaltic compositions;[15−17] however, most are high in silica content, giving the deposit a characteristic color, mineralogy, and high viscosity, which can lead to an extremely large footprint because of the eruption explosivity[18−21] Large explosive eruption deposits have been hypothesized to exist on Mars based on geochemical and morphological indicators[22−27] As relatively low-density pyroclasts can be dispersed extremely far on Earth and potentially even further in the martian atmosphere, a thin deposit (a biomicroenvironment) similar to the Askja section could be captured in a stratigraphic section in a very broad region of Mars but could be very difficult to identify with the resolution of satellite imagery currently available.[28,29] With the possibility of encountering a deposit such as this on Mars, understanding this type of microenvironment could be advantageous in the search for past life.

Biological Background. On Earth, variations in habitability are best understood by examining the biology directly, for example, by examining total biomass or biological activity[30,31] The use of DNA for information storage and ATP for energy storage is conserved across all terrestrial organisms.[32] Additionally, highly specific and low-limit-of-detection analytical tools are available for DNA and ATP via fluorescence and bioluminescence assays, respectively.[30,31] The researchers acknowledge that these assays and biomarkers are unlikely to be used for extraterrestrial life-finding missions because they are specifically adapted to the evolutionary history of Earth.[33] However, their ubiquity in terrestrial life and the precision analytical tools available for their analysis mean that they serve as proxies for biomass and biological activity in low-biomass samples[30,31] such as the Icelandic Plinian pumice deposits. Additionally, the community structure and diversity can be ascertained via metagenomic sequencing of DNA,[34] enabling improved understanding of whether an individual sample is ubiquitously habitable across multiple domains of terrestrial life or if a sample is dominated by a specific subset of organisms adapted to survive in a niche environment.

Mars Background. Although it now appears that Mars was once habitable,[35] whether or not it was inhabited is yet to be determined. Several future Mars exploration missions are tasked with searching for direct evidence of past Martian life. For example, NASA's Mars 2020 mission will travel to the Jezero crater, an ancient deep-basin lake that was active during Mars' most habitable period, the Noachian (∼4.0 Gya). Much of the lake's history has been inferred by the exposed surface mineralogy determined from visible/near-IR reflectance spectra and geomorphology determined by high-resolution visible imagery taken from the orbital spacecraft[36,37] At Jezero, the Mars 2020 rover will investigate and then cache a limited number of surface samples with a suite of instruments that will allow for the inference of chemistry, mineralogy, and biogenicity. Because only ∼40 samples will be collected, the Mars 2020 science team will need to carefully determine from Earth whether a sample is high priority for caching and which samples may have the highest potential for containing biosignatures. As such, the rover will be equipped with "stand-off" instruments that will help constrain chemistry and grain size (Supercam, PIXL), textures (PIXL), and organic content (SHERLOC).[38−40] In order to meet the objectives of the mission and to identify and cache samples that likely contain biosignatures, it is imperative that scientists understand (A) which geologic settings and rock types best create habitable microenvironments that preserve biosignatures and (B) what "stand-off" or "remote" measurements can be used to identify these samples when scientists cannot be on the ground. The Mars 2020 mission is one example of a future mission that will rely on the understanding of which settings are most suitable for preserving biosignatures and what remotely sensed information will help point to their existence. In the future, there will undoubtedly be many more missions that are either robotic or crewed that will rely on this information.

Microbiomes on Earth Compared to those of Mars. One of the main goals of biosignature-related Mars analogue research is to investigate microbial mineral preference/microbial weathering that might leave traces of organics or biotically produced secondary minerals[41] that can be used to inform biosignature detection, in a manner that might also be possible on Mars. Earth analogue sites used in astrobiology research share some of the extreme conditions found on extraterrestrial planets and moons, but in almost all cases, these sites also contain niches, conditions, or nutrients, which we would not expect to find elsewhere in our solar system. The volcanic highlands of Iceland are unvegetated, basaltic, and icy like Mars but are relatively less extreme because of the presence of higher atmospheric pressure, liquid water, and deposition of organic carbon from elsewhere.

Distinguishing which sediment microbial community members have biosignature-relevant or Mars-relevant metabolisms

https://dx.doi.org/10.1021/acsearthspacechem.0c00015
ACS Earth Space Chem. XXXX, XXX, XXX−XXX

is beyond the scope of amplicon sequencing. In this study, we have used low abundance as a rough proxy for astrobiological relevance; highest abundance species are more likely to be responding to the availability of moisture or CHNOPS, which even in these "extreme" environments are significantly higher than those found on Mars. Thus, assessing the microbial community as a whole, we have divided the microbiome into two categories: core (high abundance, >1%) versus rare (low abundance) microbes.[42−44] Often, microbial specialists that weather or degrade a recalcitrant nutrient source are found within the rare microbiome.[45] Rare microbes also might be more likely to have chemolithotrophic metabolisms similar to those possible on an extraterrestrial body such as Mars; see ref 46.

In addition, as a microbial habitat transitions from temperate to extreme conditions and the microbial community structure shifts to adapt, it is the previously rare species that generally become the core species of the new microbiome.[47] No life has so far been found on Mars, and current consensus is that although microbial life may not now exist there, it may have been present when the planet's climate was milder. As Mars' magnetic field and tectonic activity dissipated and Mars likely transitioned from warmer and wetter to drier and colder conditions,[48] previously rare microbial species likely would have survived the longest and therefore formed the most recent biosignatures of Martian life. Examining the rare microbiome and its relationship to mineral properties in a Martian analogue such as Iceland, which might reflect conditions present during Mars' early transition to a sterile cold world, can give us clues as to which mineral conditions might host traces of similar life on Mars. In this study, we compare physical parameters with the microbial community in an unaltered volcanic deposit.

METHODS

Sample Collection. A single outcrop exposing a gradation of volcanic layers was selected several kilometers away from the Askja volcano (Figure 1). The outcrop is about 0.75 m thick and is exposed along a 100 m swath that abuts a lava flow margin (Figure 2A). The low angle of the slope allows for the exposure of about 2 m of distinctly layered explosive volcanic deposits.

We collected eight samples across three transects, which were about 1.5 m apart along the outcrop (Figure 2B). The bottom two samples were collected from the sandur (samples EET-1 and 2; Figure 2C). Three samples (samples EET-4, 5, and 6; Figure 2C) were collected from the extremely fine-grained white ash of the lower C layer.[6,11] Two samples were collected from the more coarse-grained, slightly darker fall deposit (upper C) that contains pumice clasts and aeolian basaltic sand (samples EET-7 and 8; Figure 2C). The sample EET-3 was a transitional sample that contained materials from layers both above and below.

Sampling was completed with extreme care using sterile gloves, arm guards, and masks to prevent microbial contamination from the hands, arms, trowels, and respiratory systems of the sample collector. Samplers also positioned themselves downwind to minimize cross-contamination between samples. All surfaces were resterilized with ethanol between samples. The top ∼3 mm of the material was removed to avoid immediate aeolian contamination. Each sample was excavated 1−5 cm down. A total of ∼50 mL of the material was sealed in a sterile plastic tube and stored in a cooler during transport to the laboratory where the ATP assay was conducted.

"Standoff" Mineralogy. Visible and near-infrared (VNIR) (defined here as roughly 350−2500 nm) reflectance measurements are sensitive to minerals that contain transition metals,

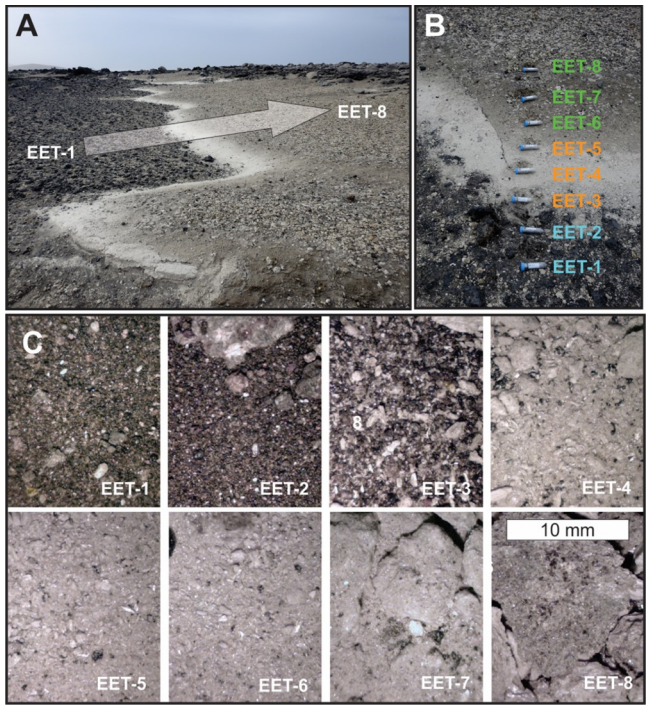

Figure 2. Field location including view of the transect of the older dark aeolian material below the white younger Askja deposit (A). Exact sampling locations (B) and close-up images of each sample (C).

such as pyroxenes, and various forms of hydration (OH^- and H_2O in phyllosilicates, e.g.) and can be used to identify the presence of these phases, even if present at low concentrations. In order to put constraints on the composition of the surface from a distance, we used an Analytical Spectral Devices (ASD) FieldSpec Halo portable mineral identifier containing an internal broad-spectrum halogen light source. External white reference calibration was performed after the instrument warmed up for at least 15 min and an internal reference was checked after every five collections. Each spectrum collected was an average of 100 scans. An area immediately adjacent to the collection site was used for ASD analysis; care was taken to ensure that the top layer of this area was undisturbed and that the area was similar in physical properties (grain size, color, etc.) to the sample collection site.

Moisture Content and Grain Size Analysis. Moisture content of ∼70 mL of the sample was measured by subtracting the dry mass from the collected mass. To obtain the dry mass, samples were dried in a convection oven at 100 °C for 5 days. After weighing the total sample, the dried sediment was passed through a set of sieves with mesh sizes of 2, 0.85, and 0.425 mm. Each grain size group was weighed, and the mass was divided by the total, giving the mass percent. The sieved fractions of EET-1, 5, and 7 were photographed and analyzed for roundness with the program ImageJ.

ATP Analysis. All samples were analyzed within 24 h of collection. An ATP bioluminescence assay kit HSII (Roche Diagnostics Ltd) was used to quantify the ATP in the samples. The samples were crushed and homogenized in double-layered, sterile plastic bags (Whirl-Pak) using a sterilized foil-covered hammer. Tris-EDTA buffer (1 mL of 100 mM TRIS, 4 mM EDTA) was added to ∼0.5 mL of the weighted sample each in triplicate and then boiled for 5 min to lyse cells. The suspension was cooled to room temperature and assayed with the ATP kit. A HY-LiTE 2 luminometer (Merck, VWR International Ltd) was used to quantify the luminescence. A standard curve was

https://dx.doi.org/10.1021/acsearthspacechem.0c00015
ACS Earth Space Chem. XXXX, XXX, XXX−XXX

Table 1. Physical Characteristics and ATP Activity of Samples Including the Mass Fractions of Different Grain sizes, the Mass Fraction of Moisture Loss after Heating, and the Bulk Geochemistry in Weight %

			EET-8	EET-7	EET-6	EET-5	EET-4	EET-3	EET-2	EET-1
Grain Size	> 2 mm (mass %)	Avg	41.6	33.6	12.3	4.9	2.5	6.1	13.7	3.5
		Std dev	16.2	3.3	4.1	3.1	1.7	1.6	9.1	1.2
	0.85-2 mm (mass %)	Avg	11.6	9.4	4.0	5.4	9.8	12.8	5.0	7.6
		Std dev	4.1	1.8	1.4	1.0	2.0	2.3	0.4	1.4
	0.425-0.85 mm (mass %)	Avg	7.8	4.4	8.0	6.6	13.2	9.2	5.7	7.8
		Std dev	2.8	0.5	8.1	0.9	0.8	0.8	0.4	0.4
	<0.425 mm (mass %)	Avg	39.1	52.6	75.7	83.1	74.5	71.9	75.6	81.0
		Std dev	9.8	1.8	4.1	1.4	2.4	2.9	8.6	1.7
Circularity		Avg	-	0.57	-	0.54	-	-	-	0.75
		Std dev	-	0.19	-	0.20	-	-	-	0.17
Roundedness		Avg		0.56		0.58				0.69
		Std dev		0.19		0.18				0.17
Moisture content	Lab (mass %)	Avg	7.9	24.1	19.7	12.8	7.2	3.5	1.2	1.3
		Std dev	1.9	1.5	1.0	0.2	0.4	1.4	0.2	0.2
SiO_2			62.51	66.71	71.06	66.22	69.07	58.60	50.52	51.32
TiO_2			1.39	1.17	0.96	1.04	1.06	1.57	1.94	1.92
Al_2O_3			13.61	13.27	12.78	17.75	12.93	13.93	14.60	14.53
FeO*			8.06	6.38	4.71	4.40	5.58	9.40	12.49	12.32
MnO			0.16	0.14	0.12	0.10	0.13	0.18	0.21	0.21
MgO			3.05	2.05	1.16	1.43	1.57	4.29	6.43	6.05
CaO			6.32	4.73	3.19	3.62	3.83	7.87	11.00	10.65
Na_2O			3.23	3.51	3.65	3.26	3.65	2.87	2.26	2.37
K_2O			1.46	1.86	2.22	2.01	2.05	1.09	0.34	0.42
P_2O_5			0.21	0.20	0.15	0.18	0.14	0.20	0.20	0.20
Total			98.88	97.81	97.88	90.44	98.21	98.60	98.59	99.05
ATP	g ATP/g sample	Avg	1.07E-10	2.23E-10	2.21E-10	4.96E-10	5.07E-10	7.26E-10	1.07E-09	1.07E-09
		Std dev	4.08E-11	4.18E-11	2.09E-11	4.58E-11	1.38E-10	1.19E-10	2.55E-10	1.08E-10

established using known standards of pure ATP in buffer prepared and analyzed on the same day with the same reagents.

Extraction and Analysis of DNA Sequencing Data. DNA was extracted from transect sediment samples in triplicate using a low-biomass protocol developed for MOBIO's PowerSoil kit.[49] DNA concentrations were measured using a Qubit 2.0 fluorimeter (Invitrogen) and Qubit quantitation kits. Reads were scaled to the lowest number of reads of any sample and sequence numbers were transformed to percent abundance. Percent abundance of phyla and proteobacterial classes was calculated for each transect position and one-way ANOVAs with Benjamin−Hochberg correction were used to test for differences in abundance among mineralogical and geochemical gradients.

Statistical Analysis of Microbial Community Correlation with Geochemistry. To examine changes in the microbial community with mineralogy, microbial community members [i.e., amplicon sequence variants (ASVs)] were divided into four categories by percentage of total sequences representing each member:

1. Core microbiome (>1% and present in >20% of samples)
2. High-abundance microbiome (>0.1%)
3. Medium-abundance microbiome (high-abundance microbiome excluding members of the core microbiome)
4. Rare microbiome (<0.1%)[42−44]

One-way PERMANOVA with Bray−Curtis and Unifrac distance measures was used to test which environmental variables significantly predicted variation in the microbial community members both overall and in each abundance category. The relative percentages of sequences belonging to rare ASVs versus core ASVs along the transect were also tested.

To further explore how the rare microbiome was shifting with mineralogy, a differential count analysis using the DESeq2 package[50] was performed to identify ASVs in the rare microbiome responsible for that shift, using the SiO_2 XRF fraction as a proxy for all mineralogy changes. The ASVs were summed at the genus, family, order, and class level and DESeq2 was reperformed to evaluate any large-scale taxonomic shifts.

Bulk Geochemical Analysis. The major elemental geochemistry was analyzed for the whole rock samples by X-ray fluorescence at Washington State University Geoanalytical Lab. The remainder of the material after DNA analysis in the triplicate sample tubes was combined, powdered, fused with lithium tetraborate in graphite crucibles in a muffle furnace, repowdered, and refused into 3 cm discs. The smaller discs were used because of limited mass of the material remaining after biological analyses. The error for this method is better than 0.001 wt. % at the 2σ envelope for all analyzed elements as reported by Geoanalytical Lab.

RESULTS

Sample Descriptions and Bulk Geochemical Analysis. Samples contained differing proportions of volcanic ash, scoria, pumice, and aeolian sediment. The stratigraphically lowest and oldest samples (EET-1 through 3) contained the most scoria and aeolian sediment. The highest proportion of fine-grained ash was in EET-4 and 5. Upsection, samples EET-6 through 8 contained increasing amounts of pumice. The normalized oxide wt % of the samples collected is presented along with the totals in Table 1. Major elemental totals were between 97.81 and 99.05 wt % for all samples except EET-5, which had a total of 90.44 wt %. The lowest total was due to the loss of volatile

https://dx.doi.org/10.1021/acsearthspacechem.0c00015
ACS Earth Space Chem. XXXX, XXX, XXX−XXX

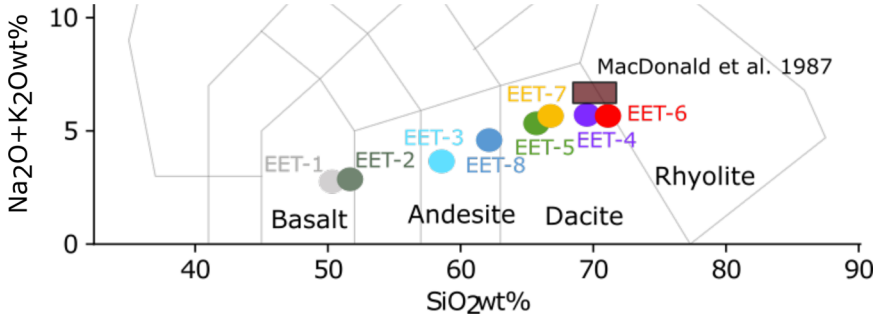

Figure 3. Bulk geochemical compositions of each sample plotted on the total alkali−silica diagram. Bulk analysis of Layer C in brown box.

species (Cl and SO_3) during the process of fusing the samples into discs, and hence, the values for EET-5 should be considered subquantitative and not directly comparable to the rest of the analyses. The stratigraphically lowest samples (EET-1 and 2) are the most mafic (highest FeO wt %) and have basaltic compositions, whereas EET-6 has the most felsic compositions (highest SiO_2 wt %) and falls close to the rhyolite field on a total alkali−silica diagram (Figure 3). Samples EET-3 and 8 are andesitic in average composition as they have mixtures of both mafic and felsic materials, whereas EET-4, 5, and 7 are dacitic.

VNIR Characteristics. Reflectance spectra in the visible to near-infrared wavelengths (300−2500 nm) show absorptions centered around 1400 and 1900 nm consistent with H_2O and OH, respectively, and an absorption around 2100 nm consistent with Si−OH bonds and a broad absorption in the 1100 nm region also consistent with silica (Figure 4). The narrow 1400

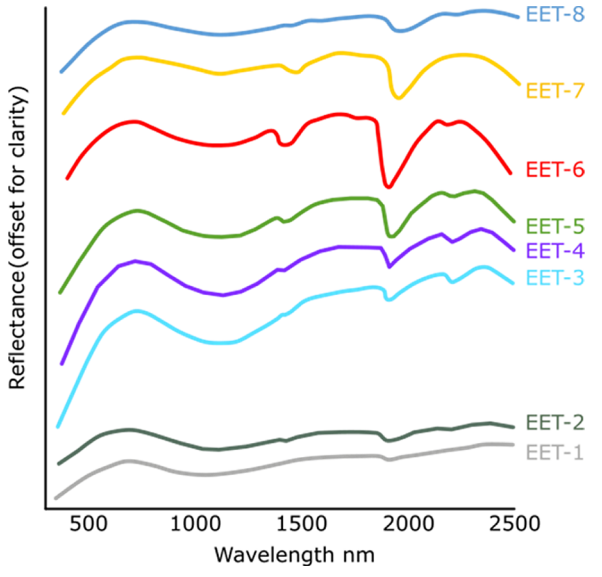

Figure 4. Spectral characteristics of the visible near-infrared (VNIR) of the samples, offset for clarity.

and 1900 nm absorptions were deepest in EET-6 and 7, while EET-3 and 4 showed the strongest absorption at ∼2100 nm. A shift to longer wavelengths in the 1100 range from 1110 to 1170 nm can be seen up the transect (Figure 4). These absorptions are captured by a set of summary parameters (Table 2) used to detect and quantify known absorptions related to specific mineral phases[51] The raw data are presented in Table S1. The summary parameters which correlate positively in the lower sandur samples (EET-1 and 2) were those associated with mafic clay minerals (e.g., BD2300, BD2165, and BD 2355) and primary minerals such as plagioclase (BD1300) and pyroxene (L and HCPINDEX). The upper Askja samples correlate with hydration indicators such as SINDEX2 and BD1900_2 (Table 2).

Grain size and Moisture Analysis. Samples included only the particles that could fit inside the sampling tube, which was ∼3 cm wide; however, there were very few clasts that were larger than that at all the sites except EET-7 and 8. These samples had larger pieces of pumice that ranged up to ∼10 cm in diameter and made up approximately 5% of the surface area of the sampling location based on imagery but were excluded from all biological and geological analyses (Figure 2, Table 1). The proportion of the two finest grain sizes (<0.85 mm) ranged from 81 to 89% in lowest samples (EET-1 through 6) with EET-5 having the higher proportion of fines in the finest grain size (<0.425 mm; Figure 5). This was in stark contrast to EET-7 and 8, which only had 56 and 46% fines, respectively. These two samples also had a much higher proportion of grains of over 2 mm in size with 33 and 42%, respectively, compared to the rest of the samples, which had less than 14% >2 mm grains. The samples with the highest moisture content were located directly above the finest grain-sized layers (Figure 5). Photos of the sieved grains of EET-1, 5, and 7 were analyzed for roundedness and an ANOVA test revealed the grains in EET-1 to be significantly more rounded (average of 0.75) than in the fresh Plinian eruptive material (average of 0.65; *F*-statistic: 8.537 on 1 and 10 DF, *p*-value: 0.01525).

ATP Analysis. The ATP measured for the transect samples ranged from 1×10^{-10} to 1×10^{-9} g per gram of sediment, with the lowest measures observed in the sample EET-1. In successive samples, ATP content increased with samples EET-4 and 5 having an average measure of 5E-10 g/g and again in samples EET-7 and 8 with an average measure near 1×10^{-9} g/g (Figure 5).

Sequencing Results. The microbial community was dominated by the class Gammaproteobacteria (25% of all sequences) and the phylum Actinobacteria (15% of all sequences), with secondary dominance of Acidobacteria, Alphaproteobacteria, and Verrucomicrobia (8−10% abundance each) (Figure 6). Almost all members of Archaea were methanogens of the phylum Euryarchaeota.

After scaling reads to the minimum number of sequences per sample, samples contained 2855 unique ASVs, <1% of which made up the core microbiome (>1% of all sequences within each sample and present in 20% or more of samples) and 70% of which made up the rare microbiome (<0.1% of all sequences within each sample). Abundant members of the microbiome included ASVs affiliated with denitrification, methylotrophy, and acetoclastic methanogenesis (Table S2).

There were four significant changes in the summed phylum abundance of the total microbiome along the transect, divided

https://dx.doi.org/10.1021/acsearthspacechem.0c00015
ACS Earth Space Chem. XXXX, XXX, XXX−XXX

Table 2. Samples Calculated Using CRISM Summary Parameters

parameter	description	rationale	EET-1-1-AVG	EET-1-2-AVG	EET-1-3-AVG	EET-1-4-AVG	EET-1-5-AVG	EET-1-6-AVG	EET-1-7-AVG	EET-1-8-AVG
		red	0.0942	0.1532	0.2731	0.2817	0.2599	0.2408	0.1603	0.1343
		green	0.0862	0.1451	0.2496	0.2606	0.2423	0.2245	0.1492	0.1241
		blue	0.0722	0.1291	0.2016	0.2157	0.2074	0.1951	0.1273	0.1046
R770	0.77 reflectance	atm dust/ice	0.0968	0.1528	0.2853	0.2914	0.2694	0.2499	0.1660	0.1383
RBR	red/blue ratio	$npFeO_x$	1.3340	1.2238	1.4122	1.3495	1.3152	1.2833	1.3010	1.3227
BD530_2	0.53 band depth	fine-grained crystalline hematite	−0.0245	−0.0222	−0.0382	−0.0366	−0.0285	−0.0209	−0.0289	−0.0303
SH600_2	0.6 shoulder height	select ferric minerals (esp. hematite and goethite)	0.0101	0.0122	0.0016	0.0026	−0.0002	−0.0004	0.0023	0.0078
SH770	0.77 shoulder height	select ferric minerals (reduced sensitivity to LCP)	0.0110	0.0089	0.0126	0.0113	0.0104	0.0106	0.0097	0.0090
BD640_2	0.64 band depth	select ferric minerals (esp. maghemite)	−0.0118	−0.0091	−0.0118	−0.0103	−0.0096	−0.0094	−0.0082	−0.0080
BD860_2	0.86 band depth	select crystalline ferric minerals (esp. hematite)	−0.0020	0.0019	0.0040	0.0032	0.0019	0.0019	0.0006	−0.0018
BD920_2	0.92 band depth	crystalline ferric minerals and LCP	0.0083	0.0073	0.0088	0.0082	0.0062	0.0054	0.0050	0.0060
BD1300	1.3 absorption	plagioclase with Fe^{2+} substitution	0.0078	0.0079	0.0024	0.0035	0.0022	−0.0035	−0.0022	−0.0002
OLINDEX3	broad 1 centered absorption	olivine	0.0234	0.0264	0.0716	0.0800	0.1109	0.1802	0.1538	0.0630
LCPINDEX2	broad 1.81 centered absorption	favors LCP	0.0276	0.0191	−0.0027	−0.0084	−0.0285	−0.0694	−0.0531	0.0032
HCPINDEX2	broad 2.12 centered absorption	favors HCP	0.0017	−0.0084	−0.0290	−0.0420	−0.0741	−0.1433	−0.1153	−0.0242
BD1400	1.4 band depth	hydrated or hydroxylated minerals	0.0002	−0.0003	0.0019	0.0009	−0.0043	−0.0106	−0.0105	−0.0026
BD1750_2	1.7 band depth	gypsum or alunite	0.0006	0.0002	−0.0009	−0.0005	−0.0005	0.0002	−0.0001	−0.00002
BD1900_2	1.9 band depth	bound H_2O except monohydrated sulfates	0.1293	0.1394	0.1338	0.1539	0.2137	0.3478	0.3192	0.1640
BD2100_2	2.1 shifted band depth	monohydrated sulfates	−0.0169	−0.0264	−0.0390	−0.0471	−0.0712	−0.1320	−0.1096	−0.0326
BD2165	2.165 band depth	pyrophillite and kaolinite group	−0.0040	−0.0055	−0.0096	−0.0105	−0.0124	−0.0200	−0.0156	−0.0067
BD2190	2.190 band depth	beidillite, allophane, and imogolite	0.0019	0.0017	0.0069	0.0042	−0.0013	−0.0126	−0.0106	−0.0006
MIN2200	2.16 and 2.21 band depth	kaolinite group	−0.0014	−0.0007	0.0029	−0.0009	−0.0104	−0.0327	−0.0279	−0.0071
BD2210_2	2.21 band depth	Al−OH minerals	0.0071	0.0087	0.0201	0.0181	0.0139	0.0082	0.0054	0.0073
D2200	2.2 micron dropoff	Al−OH minerals	0.0062	0.0094	0.0261	0.0220	0.0115	−0.0078	−0.0104	0.0021
BD2230	2.23 band depth	hydroxylated ferric sulfate	0.0012	0.0014	0.0020	0.0020	0.0012	0.0002	−0.0004	0.0006
BD2250	2.25 band depth	opal and other hydrated silica phases	0.0102	0.0106	0.0247	0.0186	0.0027	−0.0294	−0.0280	−0.0016
MIN2250	2.21 and 2.26 band depth	opal	−0.0107	−0.0037	0.0060	0.0046	−0.0002	−0.0080	−0.0114	−0.0094
BD2265	2.265 band depth	jarosite, gibbsite, acid-leached nontronite	−0.0003	−0.0017	−0.0026	−0.0042	−0.0089	−0.0193	−0.0160	−0.0064
BD2290	2.3 band depth	Mg, Fe−OH minerals	−0.0015	−0.0023	−0.0047	−0.0052	−0.0080	−0.0140	−0.0112	−0.0059
D2300	2.3 dropoff	hydroxylated Mg, Fe-silicates	−0.0186	−0.0182	−0.0248	−0.0276	−0.0360	−0.0647	−0.0540	−0.0239

https://dx.doi.org/10.1021/acsearthspacechem.0c00015
ACS Earth Space Chem. XXXX, XXX, XXX−XXX

Table 2. continued

parameter	description	rationale	EET-1-1-AVG	EET-1-2-AVG	EET-1-3-AVG	EET-1-4-AVG	EET-1-5-AVG	EET-1-6-AVG	EET-1-7-AVG	EET-1-8-AVG
BD2355	2.35 band depth	chlorite, prehnite, pumpellyte	−0.0091	−0.0107	−0.0201	−0.0210	−0.0221	−0.0257	−0.0204	−0.0084
SINDEX2	inverse lever rule at 2.29	mono- and poly-hydrated sulfates	0.0010	0.0028	0.0002	0.0081	0.0282	0.0695	0.0605	0.0189

into categories of older (EET 1 and 2), mixed (EET 3 and 4, at the transition zone), and younger Plinian parent materials (EET 5−8), after Benjamin−Hochberg p-value correction (Figure 7). Acidobacteria abundance was highest in the transition zone. Abundance of Alphaproteobacteria and Euryarchaeota was much lower in the mixed and younger samples compared to the older samples, while Planctomycetes were more abundant in the mixed and younger parent material zone.

Core microbiome relative abundance was significantly predicted by ATP concentration (i.e., biological activity; $df = 7$, pseudoF = 3.282, $p = 0.006$) and moisture content ($df = 7$, pseudoF = 2.563, $p = 0.038$) of the sediment (Table 3, Figure 7). Shift in the high-abundance microbiome was also predicted by ATP concentration. In contrast, relative abundance of the rare microbiome was not predicted by biological activity or moisture but was significantly predicted by bulk geochemistry of the sediment and by the fractional abundance of sediment grains between 425 and 850 μm (Table 3).

Phylogenetic shift (i.e., use of Unifrac distances in PERMANOVA) was only significantly predicted in medium- to high-abundance microbes (excluding the core microbiome) by the fractional abundance of sediment grains between 425 and 850 μm ($df = 7$, pseudoF = 2.295, $p = 0.018$). The abundance of certain phyla also varied greatly depending on the age of the material (Figure 8).

Differential count (DESeq2) analysis of the rare microbiome did not yield any ASVs or genera that shifted significantly from low to high silica content after Benjamin−Hochberg correction of p values—this was unsurprising given that each individual ASV was of low abundance. When summed across different taxonomic levels, the families Hydrogenophilaceae and Caulobacteraceae, both in the phylum Proteobacteria, were significantly more abundant in low-silica samples and the order Rhizobiales was significantly more abundant in high-silica samples.

DISCUSSION

Geological Observations. The Plinian eruption at Askja in 1875 produced a well-sorted fine-grained fall deposit followed by a more pumice-rich fall deposit, which we examined geochemically and mineralogically using measurements similar to those that are currently or planned to be available on Mars with robotic missions. Additionally, we examined the biological patterns associated with these deposits in an effort to inform a sampling protocol to maximize the recovery of bioindicators in volcanic terrains.

VNIR and XRF Characteristics of Explosive Eruptions. An explosive eruption on Earth often results in deposits of fine-grained glassy particles with some components of pumice and crystals. Although this determination can be made from a small sample of materials alone, it can be helpful to have micro-analytical techniques and field relationships with surrounding units.[52] As this might be limited by orbital resolution context imagery and with the narrow mobility of a rover or crewed missions to Mars, we focused our characterization of these deposits on up-close imagery, VNIR, and XRF analysis.

The color and grain size of volcanic deposits can be determined from imagery; however, the color is not specific enough to identify the chemistry of volcanic rocks. XRF measurements provide the bulk geochemical analysis of the material which, if fresh, allows for the standard classification of the rock, providing valuable information of the eruption style that produced the rock. VNIR spectra can confirm the XRF geochemical classification by identifying minerals present, which correspond to the

https://dx.doi.org/10.1021/acsearthspacechem.0c00015
ACS Earth Space Chem. XXXX, XXX, XXX−XXX

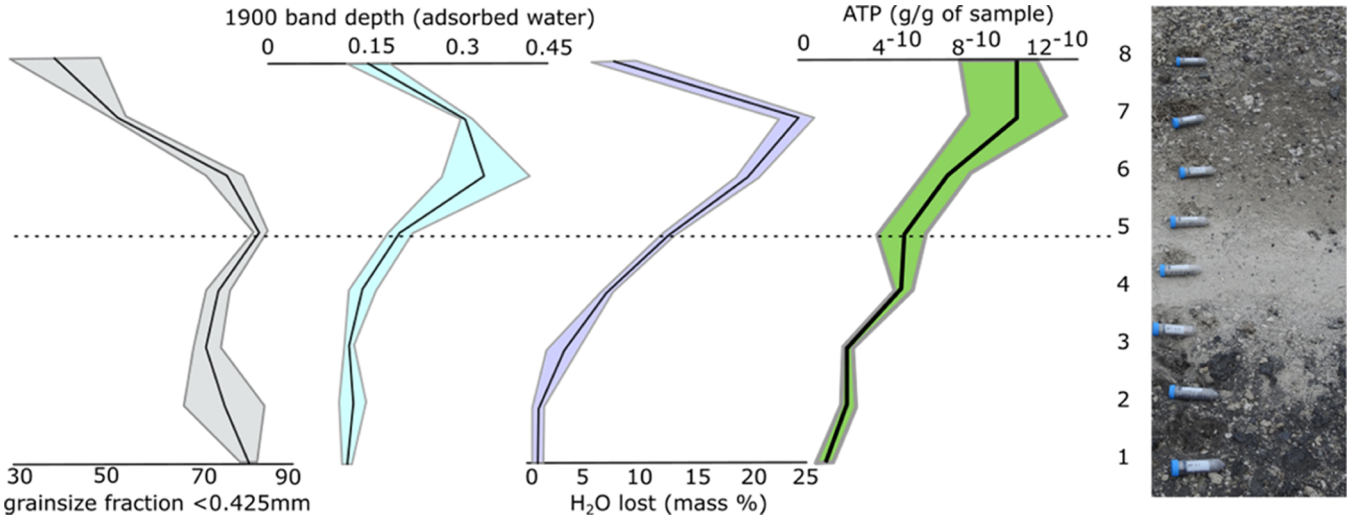

Figure 5. Grain size, water content (adsorbed and free water), and overall ATP for each sample shown next to a photo of the transect. The colored envelope represents the error with the solid line representing the average for each sample. The dashed line references sample 5 in each graph.

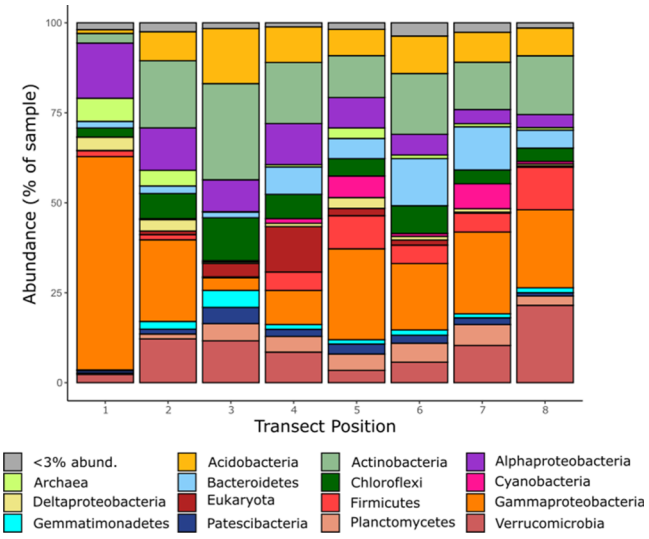

Figure 6. Relative abundances of phyla/classes after reads were scaled to the lowest number of sequences per sample.

rock type, for example, some spectral summary parameters (such as SH600_2, BD920_2, BD1300., LCPINDEX, and HCPINDEX) show a correlation for mafic minerals in the more mafic chemical compositions (Figure 9).

The Askja eruption occurred less than 200 years ago and in an area that is quite cold and dry; thus, we expected to see little evidence of alteration. The primary style of alteration captured by VNIR was in the form of slight devitrification, captured by the 1400 and 1900 nm absorptions (e.g., summary parameter BD1900_2). This process is best exemplified in the samples with higher silica content and smallest particles. Nearly all of the summary parameters which target clay minerals indicated that the older material (lowest layers in the sampled stratigraphy) had the highest content of these minerals. This higher concentration of clay minerals may have accumulated because of weathering in the older layers over time.

The bulk geochemical compositions of the 1875 Askja layer C ash and a representative ash layer are shown in Figure 3 and match samples EET-4 and EET-6 most closely,[10] although our analyses have slightly lower Na_2O wt % than the published values.

There are few igneous minerals (3% plagioclase, 2% pyroxene, and 0.5% iron oxide) in the Askja ash and pumice as most of the deposit (94.5%) is glass,[11] which suggests that the dominant factor for influencing the VNIR spectra is likely not the minerals but the FeO wt % content of the glass.[53] The VNIR signature of glass is fairly featureless but shows broad absorptions at 1100 and 1900 nm.[54] Additionally,[54] we found that an increase in FeO wt % in the glass affected the spectra in three specific ways: (1) a decrease in overall reflectance, (2) a flattening in the visible range with a near disappearance of the 800 nm shoulder, and (3) the slope between 1800 and 2400 nm will increase (Figure 10). The samples EET-5 through 8 have similar reflectance and iron content as the 100−125 and 200−180 μm grain size experiments, whereas EET-1 through 4 were more consistent with the smaller grain size experiments. This observation broadly matches the grain size data for our samples except for EET-5 which has a high proportion of small grains and EET-3 which does not. The good correlation of these data suggests that the glassiness (as opposed to the mineral content) and the degree of the mafic material are broadly responsible for the spectral characteristics seen in the VNIR range. The two major differences between our samples and the experiments were thus the likely inclusion of some crystals in the glassy matrix and wide variations in elemental oxides other than FeO (such as SiO_2), which may account for the higher reflectance of EET-4 and EET-3 for the overall iron content.

Microbial Community. The microbiome of these sediments appears to be responding to two different sets of environmental drivers. The core microbiome varies significantly with biological activity (ATP) and with free moisture (Figure 7, Table 3), while the rare microbiome varies significantly with the mineralogy and grain size of the sediment (Table 3).

The core microbiome's shift with increasing water content was probably responsible for the increase in biological activity over the transect (Figure 7). Members of the core microbiome most responsible for this shift according to FDR-corrected one-way ANOVA results include two ASVs from the phylum Bacteroidetes, family Bacteroidia: one from the candidate genus OLB8 (p = 0.02), which has also been found in a community of nitrate reducers,[55] and the other from the candidate family AKYH767 (p = 0.02) (Figure 7, Table S1). Closest environmental hits for both ASVs are associated with nitrification, denitrification, and annamox (Table S1).

https://dx.doi.org/10.1021/acsearthspacechem.0c00015
ACS Earth Space Chem. XXXX, XXX, XXX−XXX

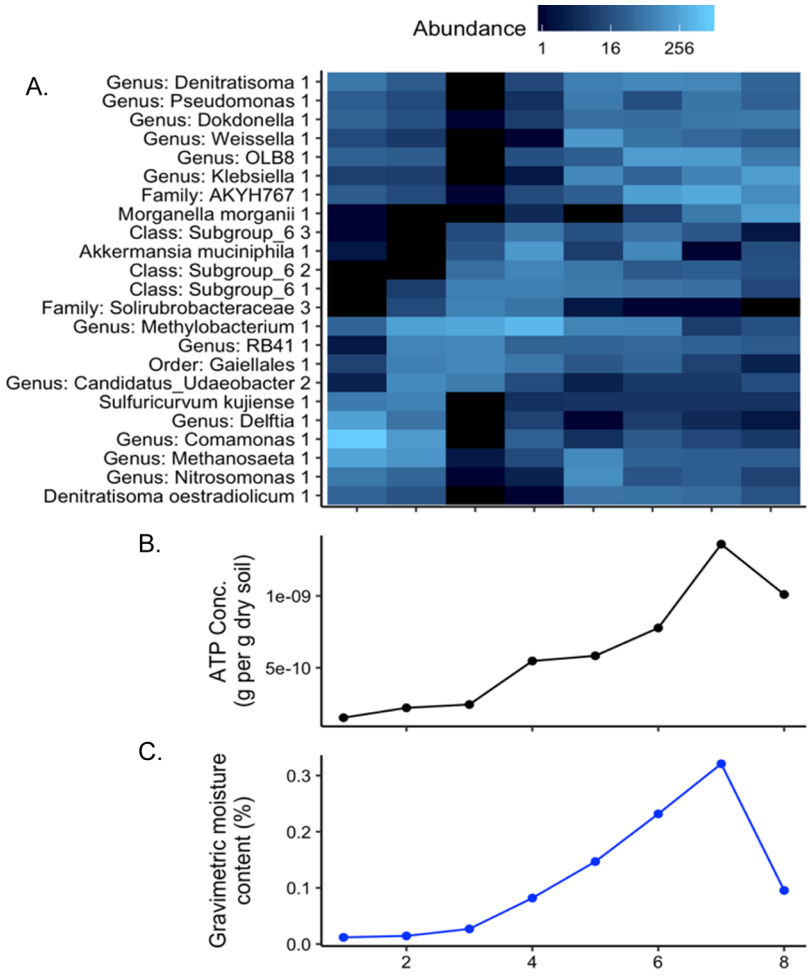

Figure 7. (A) Heat map of abundances of ASVs which were present in more than 20% of samples and were represented by more than 50 sequences per sample, when sequences are scaled to the lowest number of sequences per sample. Samples are in the order in which they were collected across a mineralogical transect. (B) ATP concentration and (C) gravimetric moisture content values across the transect.

Table 3. One-Way PERMANOVA Tests of Sediment Properties Against Different Subsets of the Full Multivariate Dataset of ASVs (Species Equivalents) in This Study[a]

variable	rare ASVs (<0.1%)	med. abun. ASVs	abundant ASVs	top ASVs	all ASVs
gravimetric moisture content	*			*	
grain size (425−850 μm)	*				
SiO_2 frac	**				*
TiO_2 frac	*				*
FeO_x frac	*				
MnO frac	*				
MgO frac	*				
CaO frac	**				
Na_2O frac	*	*	*		*
K_2O frac	*				
ATP conc. (g per g dry soil)			*	**	*

[a]Top ASVS were those present in more than 20% of samples and represented by more than 50 sequences per sample; medium-abundant ASVs were present in more than 20% of samples and which had between five and 50 representative sequences per sample; abundant ASVS were top ASVs and medium-abundance ASVs combined; and rare ASVs were those present in less than 20% of samples or represented by fewer than five sequences per sample. * indicates $p < 0.05$; ** indicates $p < 0.01$.

Changes in the total microbiome, when summed across phyla, also showed significant changes in the abundance of methanogens and methylotrophs/methanotrophs across the transect (Figure 8), with ASVs from both functional categories decreasing in abundance with decreasing age of the parent material. This was surprising; whether or not methanogens in this transect were producing methane, we would expect them to be more successful and more prevalent in more anaerobic sediments with higher water content, which describe the younger end of the transect. However, this may be due to an increase in overall organic matter accumulation with age, providing increased access to acetic acid or methanol at the older end of the transect. We also found an increase in the abundance of members of Planctomycetes along the transect with increasing moisture content. This was unsurprising because Planctomycetes have mainly been isolated from freshwater or marine environments or moist soils and sediments.[56]

Shifts in the rare microbiome are more complicated to parse but may be more relevant to the field of astrobiology. Low-abundance (rare) ASVs or OTUs have in the past often been excluded from analysis because of the prevailing belief that they are unlikely to be active, but more recent studies have found that this component of the microbiome is functionally important.[46,47] The correlation of the rare microbiome in these samples with mineralogical features of the sediment (i.e., chemical composition from XRF) (Table 3) suggests that the low-abundance community

https://dx.doi.org/10.1021/acsearthspacechem.0c00015
ACS Earth Space Chem. XXXX, XXX, XXX−XXX

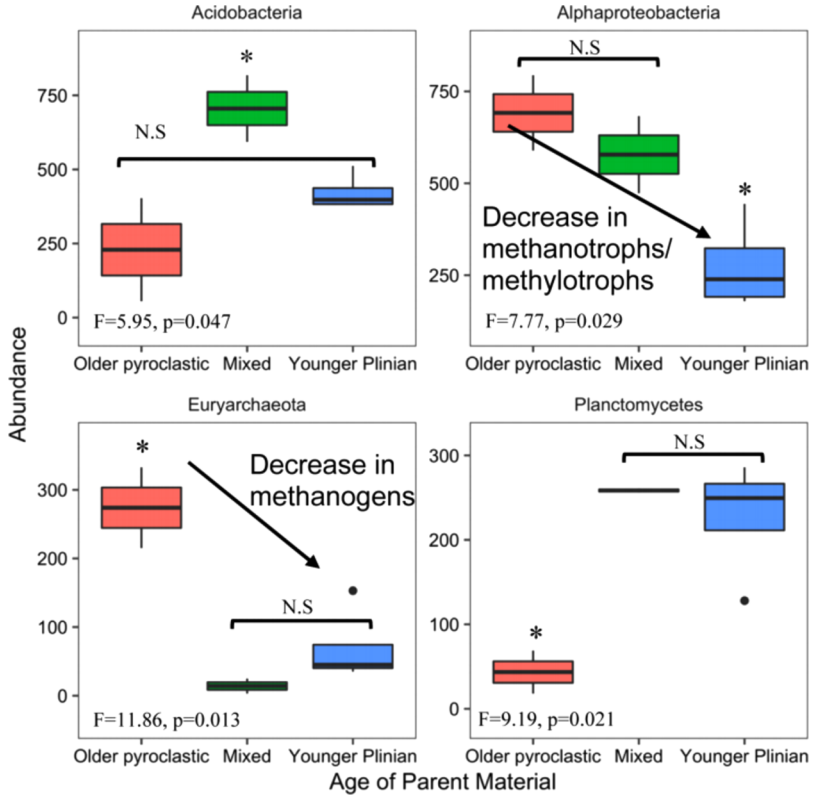

Figure 8. Phyla with significant differences in abundance with age of the parent material, as tested by one-way ANOVA with FDR p-value correction. The decrease in Alphaproteobacteria is mainly due to the decrease in one sequence for a methanotroph/methanol consumer, and the decrease in Euryarchaeota is due to the decrease in two sequences, one an acetoclastic methanogen (genus *Methanosaeta*) and the other a methanogen that can form methane from either formate or H_2 and CO_2 (genus *Methanobacterium*). Abundances are relative to the lowest biomass sample (EET-4). Stars indicate significance of $p < 0.05$, dots are outliers, and N.S. means 'not significant'.

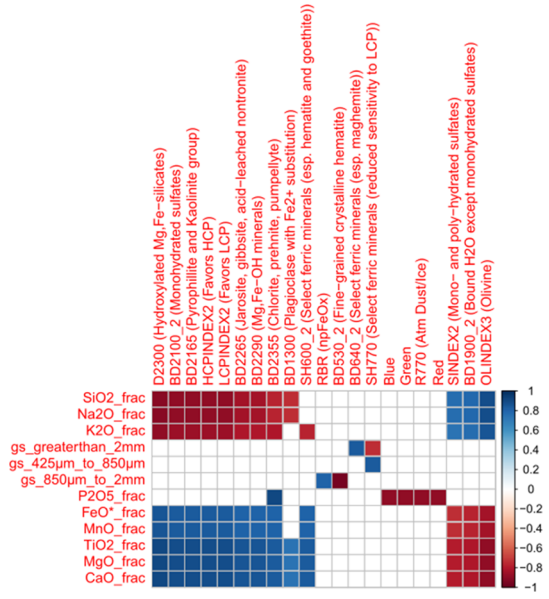

Figure 9. Spearman correlation plot comparing which CRISM spectral parameters (top) correlate with bulk geochemistry and grain size of the samples. Red indicates negative correlation and blue indicates positive correlation and white indicates no correlation.

is active and undergoes environmental selection rather than representing a nonactive portion of the detectable microbiome such as a dormant microbial seed bank or taphonomic signal (as discussed in ref 45).

This shift in the rare microbiome with change in geochemistry could be due to differing chemicals/nutrients provided by the sediment grains or the manner in which the microtopography of sand grains varies by composition. A number of studies have linked individual microbial species or bulk abundance of microbes to particular mineral materials that provide a beneficial habitat (i.e., protection from radiation or temperature and availability of moisture) such as the protected crevices of sand grains[44,57] or micronutrients weathered biotically or abiotically from rocks or minerals.[58−61] However, there are relatively few studies linking mineralogical properties of rocks and sediment to overall prokaryotic community composition in plant-free environments, and most of these studies focus on the most abundant community members. A study of prokaryotic colonization of pegmatitic granite found that different community profiles were characteristics of different mineral crystals, including community differences corresponding with varying levels of Al, Si, and Ca oxide derived from XRF readings.[62] The endolithic microbial community structure in Atacama has been linked to the rock porosity/physical structure rather than mineral chemistry and light transmission properties, as water retention by rocks was the most important factor for colonization.[63] In two studies of microbial colonization in sand grains of marine sediment exposed to mechanical abrasion, prokaryotes grew preferentially in concave areas and crevices and were mostly not found on smooth or convex surfaces.[44,57] Probandt et al. found that differences between the microbiome of individual sand grains were mainly due to the presence of rare species and each sand grain was not significantly different from the bulk sediment once rare species were removed.[44]

https://dx.doi.org/10.1021/acsearthspacechem.0c00015
ACS Earth Space Chem. XXXX, XXX, XXX−XXX

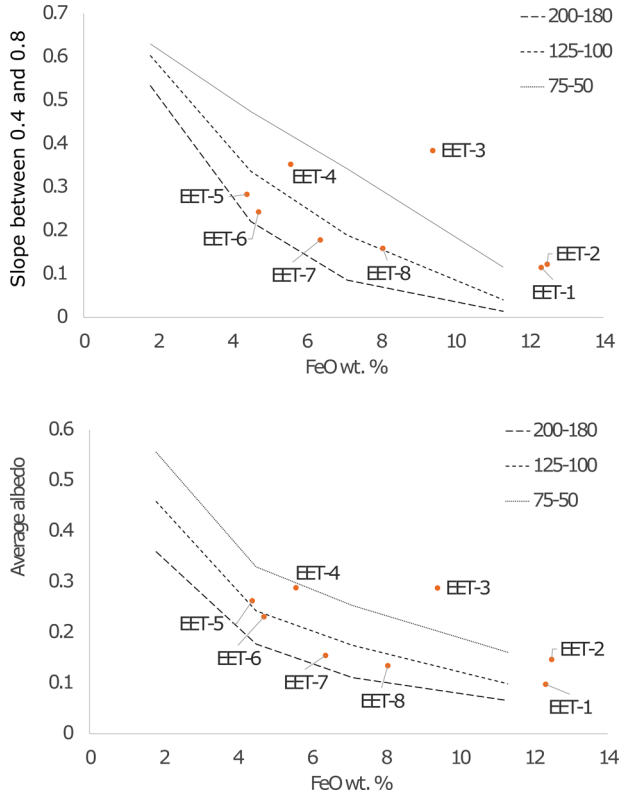

Figure 10. Graph illustrating the relationship between FeO content, grain size, and average spectral characteristics of glass. The grain size of experimental glass powders from Carli et al.[53] is in mm and is represented by lines of different patterns. Our samples, which are mixtures of grain sizes, are the orange dots.

Over the compositional gradient at Askja, only the rare microbiome shifted in community composition (i.e., relative abundance of individual ASVs) with changes in geochemistry. This shift was correlated with the proportion of grains of the size 425−850 μm. This shift may be due to the presence, or lack thereof, of crevices for microbes to occupy in this particular grain size. Common eruption products of Plinian eruptions include rocks that have increased porosity (pumice) and poorly rounded grains (ash fall).

Relationship between the Grain Size and Shape and Favorable Habitat. The two factors unrelated to geochemistry that affected the microbial communities were the presence of water and the proportion of rounded grains. Both of these factors are related to the volcanic nature of the sediment. The samples which are older and contain more wind-blown materials (EET-1 through 3) are likely to contain more rounded grains because of the bumping and grinding that grains experience when bouncing over the landscape. Conversely, the young airfall deposits (EET-4 through 8) are more likely to retain their crevices as the deposition process of volcanic ash and pumice is relatively gentle. Thus, fresh volcanic products that have not been remobilized could be a particularly good habitat.

Additionally, the fine-grained compacted ash layer (EET-4 and EET-5) may be serving as an aquitard, allowing water to be trapped in the more porous layers above. Thus, eruptions which progressed similar to the Askja 1875 eruption (highly explosive and transitioning from ash into more pumice-rich, common in Plinian-style eruptions) are capable of rapidly creating a nonrounded, water storing, and protective habitat that may be laterally very expansive although not particularly thick.

Implications for Targeted Sampling on Mars. Mars' early volcanic history may have been defined by more explosive volcanism as evidenced by older regolith that is poorly consolidated and fine-grained.[22,25,64,65] Most of these eruptions are chemically basaltic in nature, similar to several eruptions preserved on Earth such as Sunset Crater 1085 CE, Etna 122 BCE, Colima 1913, or the Fontana unit 30 kya[17,66−68] There is also evidence for a widespread ash deposit in the Nili Fossae and Jezero crater region, where the Mars 2020 rover will search for evidence of biosignatures, stemming from the Syrtis Major volcanic province.[27] Additionally, there is evidence from the Compact Reconnaissance Imaging Spectrometer for Mars (CRISM) spectral imager that this reported ash layer is associated with clay mineralogy.[69]

The preservation of biological traces of chemoautotrophic and chemoorganotrophic communities in volcanic sediments in early Archaean fossils such as the Kitty's Gap Chert suggests that if similar organisms existed in water-saturated volcanoclastic environments on Mars, their traces would also have been preserved, although their identification would likely require sample return.[70] This is a promising avenue for biosignature investigation as it is possible that Mars' window of habitability may not have been long enough for photosynthesis to develop;[71,72] without the gross primary production rates provided by photosynthesis, it would be unlikely that a rover could detect definitive biosignatures such as large organic deposits or macrofossils.

Given our observations and interpretation of samples from the Askja eruption, a mission that has similar instrumentation to this study and the objective of searching for biosignatures should prioritize samples that show evidence for fine-grained deposits underlaying a pumaceous air-fall. Our work shows that grains or clasts that have been deposited in place with limited remobilization, which would increase smoothness and decrease crevices and protected niches, should be prioritized. Composition is perhaps less of a driving factor than the physical nature of the deposits and the associated geologic history.

Although the focus of our research was on a specific volcanic analogue, the chemical and physical properties we studied are universally variable within nearly all environments on Mars. Thus, our findings can be used to guide astrobiological sampling more broadly. For example, the juxtaposition of water and fine-grained particles could occur from subsurface disturbances of Martian sediment,[73−76] or adsorbed water may signify regions which likely contain near-surface aqueous activity.[77,78] Furthermore, our findings could be paired with measured data from Mars[79] and recommendations of environments with high likelihood of preservation[80] to maximize abundance of past life. Our results also suggest that small gradations over geological layers have a significant effect on which microbial community members are present. Sampling across such sedimentary gradients on Mars would provide a much wider variety of possible biosignatures and therefore a much greater likelihood of detecting life."

■ CONCLUSIONS

By investigating analogous environments on Earth using the same instrumental capabilities available to planetary surface missions, we are able to devise a sampling protocol that is likely to maximize biosignature payloads. Surfaces that appear homogenous at large scales may contain a huge variety of microenvironments and will need further investigation to select high-return sampling sites. This study illustrates how sites can be narrowed down using geological relationships and "stand-off" techniques that require little sample preparation and have a fast turn-around time for results.

https://dx.doi.org/10.1021/acsearthspacechem.0c00015
ACS Earth Space Chem. XXXX, XXX, XXX−XXX

We chose a single small site that had several overlapping gradients (geochemical, grain size, hydrologic, and age) to illustrate the relative importance of these features and test how these features may be studied using analytical capabilities on Mars. We confirmed that overall biological activity correlates with free water in the sample and is linked to a core community including aerobic heterotrophs and putative denitrifiers, methanogens, and methylotrophs/methanotrophs. When excluding highly abundant ASVs (which include unlikely phyla for Mars) from our dataset, we see changes in the microbial community that respond to geological differences in the substrates. Specifically, grain size, geochemistry, and deposit age/degree of transport affect the abundance and composition of the microbiome, which may have implications for sampling missions.

Additionally, whereas the absolute age of the geologic units is fairly inconsequential, the depositional history of the two units leads to a greatly varied habitat. The older deposit was composed of wind-blown grains which are more rounded compared to the younger fall deposit above. Protected crevices in grains are common in Plinian eruption deposits of all chemical compositions and thus should be sought out on sampling missions. Based on these results, we recommend two sets of sampling protocol:

1. A protocol to target highest levels of diversity and abundance should look for fresh Plinian fall deposits with any sort of chemical gradient which can be identified using VNIR at distance, confirmed with XRF and imagery at close range.

2. Further success could result from finding a sequence of deposits with very fine grain size directly underneath more pumaceous fall deposits, thus creating a small local aquifer directly below a porous habitat. This suggests that the deposit thickness might be an important factor when scanning for the ideal habitat.

■ ASSOCIATED CONTENT

Supporting Information

The Supporting Information is available free of charge at https://pubs.acs.org/doi/10.1021/acsearthspacechem.0c00015.

Raw visible near-infrared data for EET 1 through 8 (XLSX)

Top 12 most abundant ASVs and their percent of total reads, with their SILVA database genus assignment and NCBI nucleotide database top environmental and culture hits for the sequence of that ASV (PDF)

■ AUTHOR INFORMATION

Corresponding Author

Amanda Stockton − *Department of Chemistry and Biochemistry, Georgia Institute of Technology, Atlanta, Georgia 30332, United States;* orcid.org/0000-0002-0306-1760; Email: astockto@gatech.edu

Authors

Erika Rader − *Department of Geological Sciences, University of Idaho, Moscow, Idaho 83844, United States;* orcid.org/0000-0003-2729-4275

Anna Simpson − *Department of Chemistry and Biochemistry, Georgia Institute of Technology, Atlanta, Georgia 30332, United States*

Elena Amador − *Jet Propulsion Laboratory, California Institute of Technology, Pasadena, California 91109, United States*

Julia M. Fraser − *Department of Chemistry and Biochemistry, Georgia Institute of Technology, Atlanta, Georgia 30332, United States*

Samuel Holtzen − *Department of Chemistry and Biochemistry, Georgia Institute of Technology, Atlanta, Georgia 30332, United States*

Ashley Hanna − *Department of Chemistry and Biochemistry, Georgia Institute of Technology, Atlanta, Georgia 30332, United States*

Morgan L. Cable − *Jet Propulsion Laboratory, California Institute of Technology, Pasadena, California 91109, United States;* orcid.org/0000-0002-3680-302X

Thomas Cullen − *Centre for Autonomous and Cyberphysical Systems, Cranfield University, College Road MK43 0AL, U.K.*

Zach Duca − *Department of Chemistry and Biochemistry, Georgia Institute of Technology, Atlanta, Georgia 30332, United States*

Diana Gentry − *Biospheric Science Branch, NASA Ames Research Center, Mountain View, California 94035, United States*

Gayathri Murukesan − *Department of Biochemistry/Biochemistry, University of Turku, Turku 20500, Finland*

Vincent Rennie − *School of Environment, Earth and Ecosystem Sciences, Open University, Milton Keynes MK7 6AA, U.K.*

Adam H. Stevens − *UK Centre for Astrobiology, School of Physics and Astronomy, University of Edinburgh, Edinburgh EH9 3FD, U.K.*

Scot Sutton − *Department of Chemistry and Biochemistry, Georgia Institute of Technology, Atlanta, Georgia 30332, United States*

George Tan − *Department of Chemistry and Biochemistry, Georgia Institute of Technology, Atlanta, Georgia 30332, United States*

David Cullen − *Centre for Autonomous and Cyberphysical Systems, Cranfield University, College Road MK43 0AL, U.K.*

Wolf Geppert − *Department of Molecular Physics, Stockholm University, Stockholm SE-106 91, Sweden*

Complete contact information is available at: https://pubs.acs.org/10.1021/acsearthspacechem.0c00015

Notes

The authors declare no competing financial interest.

This Targeted Locus Study project has been deposited at DDBJ/EMBL/GenBank under the accession KEEJ00000000. The version described in this paper is the first version, KEEJ01000000.

■ ACKNOWLEDGMENTS

We would like to acknowledge the funding sources that allowed us to gather and analyze these data: NASA award #NNX16AK13G, the NASA Postdoctoral Program, Georgia Institute of Technology, and the state of Georgia. Permitting was provided by the Icelandic Centre for Research, Icelandic Institute of Natural History, and Vatnajökull National Park. Some work was done at the Georgia Institute of Technology (Georgia Tech) with financial support from the State of Georgia, USA. This work was performed in part at the Georgia Tech Institute for Electronics and Nanotechnology, a member of the National Nanotechnology Coordinated Infrastructure (NNCI), which is supported by the National Science Foundation (Grant ECCS-1542174). Some of the research was carried out at the Jet Propulsion Laboratory, California Institute of Technology, under a contract with the National Aeronautics and Space Administration (80NM0018D0004).

■ ABBREVIATIONS

VNIR, visible near-infrared; XRF, X-ray fluorescent; EET, Elena's experimental transect; ATP, adenosine triphosphate;

PIXL, Planetary Instrument for X-ray lithochemistry; SHERLOC, Scanning Habitable Environments with Raman & Luminescence for Organics & Chemicals; NASA, National Aeronautics and Space Administration; DNA, deoxyribonucleic acid; ASD, Analytical Spectral Devices; EDTA, ethylenediaminetetraacetic acid; qPCR, quantitative polymerase chain reaction; ASV, amplicon sequence variants; ANOVA, analysis of variance; PERMANOVA, permutational multivariate analysis of variance

REFERENCES

(1) Arnalds, O.; Dagsson-Waldhauserova, P.; Olafsson, H. The Icelandic volcanic aeolian environment: Processes and impacts—A review. *Aeolian Res.* **2016**, *20*, 176−195.

(2) Arnalds, O. Dust Sources and Deposition of Aeolian Materials in Iceland. *Icel. Agric. Sci.* **2010**, *23*, 3.

(3) Arnalds, O.; Gisladottir, F. O.; Orradottir, B. Determination of aeolian transport rates of volcanic soils in Iceland. *Geomorphology* **2012**, *167−168*, 4−12.

(4) Thordarson, T.; Höskuldsson, Á. Postglacial volcanism in Iceland. *Jökull* **2008**, *58*, No. e228.

(5) Edgett, K. S.; Lancaster, N. Volcaniclastic aeolian dunes: Terrestrial examples and application to Martian sands. *J. Arid Environ.* **1993**, *25*, 271−297.

(6) Sparks, R. S. J.; Wilson, L.; Sigurdsson, H. The pyroclastic deposits of the 1875 eruption of Askja, Iceland. *Philos. Trans. R. Soc., A* **1981**, *299*, 241−273.

(7) Hartley, M. E.; Thordarson, T.; de Joux, A. Postglacial eruptive history of the Askja region, North Iceland. *Bull. Volcanol.* **2016**, *78*, 28.

(8) Carey, R. J.; Houghton, B. F.; Thordarson, T. Tephra dispersal and eruption dynamics of wet and dry phases of the 1875 eruption of Askja Volcano, Iceland. *Bull. Volcanol.* **2010**, *72*, 259−278.

(9) Huntingdon-Williams, A. G. Total grain size distribution and morphology characteristics of the Askja 1875 C tephra. Doctoral Dissertation, University of Iceland, 2018.

(10) Macdonald, R.; Sparks, R. S. J.; Sigurdsson, H.; Mattey, D. P.; McGarvie, D. W.; Smith, R. L. The 1875 eruption of Askja volcano, Iceland: combined fractional crystallization and selective contamination in the generation of rhyolitic magma. *Mineral. Mag.* **1987**, *51*, 183−202.

(11) Sigurdsson, H.; Sparks, R. S. J. Petrology of rhyolitic and mixed magma ejecta from the 1875 eruption of Askja, Iceland. *J. Petrol.* **1981**, *22*, 41−84.

(12) Mountney, N. P.; Russell, A. J. Sedimentology of cold-climate aeolian sandsheet deposits in the Askja region of northeast Iceland. *Sediment. Geol.* **2004**, *166*, 223−244.

(13) Walker, G. P. L. Explosive volcanic eruptions—a new classification scheme. *Geol. Rundsch.* **1973**, *62*, 431−446.

(14) Walker, G. P. L. Plinian eruptions and their products. *Bull. Volcanol.* **1981**, *44*, 223.

(15) Walker, G. P. L.; Self, S.; Wilson, L. Tarawera 1886, New Zealand—a basaltic plinian fissure eruption. *J. Volcanol. Geotherm. Res.* **1984**, *21*, 61−78.

(16) Williams, S. N. Plinian airfall deposits of basaltic composition. *Geology* **1983**, *11*, 211−214.

(17) Coltelli, M.; Del Carlo, P.; Vezzoli, L. Discovery of a Plinian basaltic eruption of Roman age at Etna volcano, Italy. *Geology* **1998**, *26*, 1095−1098.

(18) Sigurdsson, H.; Houghton, B.; McNutt, S.; Rymer, H.; Stix, J. *The Encyclopedia of Volcanoes*; Elsevier, 2015.

(19) Gualda, G. A. R.; Ghiorso, M. S. The Bishop Tuff giant magma body: an alternative to the Standard Model. *Contrib. Mineral. Petrol.* **2013**, *166*, 755−775.

(20) Jensen, B. J. L.; Pyne-O'Donnell, S.; Plunkett, G.; Froese, D. G.; Hughes, P. D. M.; Sigl, M.; McConnell, J. R.; Amesbury, M. J.; Blackwell, P. G.; van den Bogaard, C.; Buck, C. E.; Charman, D. J.; Clague, J. J.; Hall, V. A.; Koch, J.; Mackay, H.; Mallon, G.; McColl, L.; Pilcher, J. R. Transatlantic distribution of the Alaskan white river ash. *Geology* **2014**, *42*, 875−878.

(21) Myers, M. L.; Wallace, P. J.; Wilson, C. J. N.; Watkins, J. M.; Liu, Y. Ascent rates of rhyolitic magma at the onset of three caldera-forming eruptions. *Am. Mineral.* **2018**, *103*, 952−965.

(22) Hynek, B. M.; Phillips, R. J.; Arvidson, R. E. Explosive volcanism in the Tharsis region: Global evidence in the Martian geologic record. *J. Geophys. Res.: Planets* **2003**, *108*, 5111.

(23) Kerber, L.; Head, J. W.; Madeleine, J.-B.; Forget, F.; Wilson, L. The dispersal of pyroclasts from ancient explosive volcanoes on Mars: Implications for the friable layered deposits. *Icarus* **2012**, *219*, 358−381.

(24) Michalski, J. R.; Bleacher, J. E. Supervolcanoes within an ancient volcanic province in Arabia Terra, Mars. *Nature* **2013**, *502*, 47−52.

(25) Bandfield, J. L.; Edwards, C. S.; Montgomery, D. R.; Brand, B. D. The dual nature of the martian crust: Young lavas and old clastic materials. *Icarus* **2013**, *222*, 188−199.

(26) Morris, R. V.; Vaniman, D. T.; Blake, D. F.; Gellert, R.; Chipera, S. J.; Rampe, E. B.; Ming, D. W.; Morrison, S. M.; Downs, R. T.; Treiman, A. H.; Yen, A. S.; Grotzinger, J. P.; Achilles, C. N.; Bristow, T. F.; Crisp, J. A.; Des Marais, D. J.; Farmer, J. D.; Fendrich, K. V.; Frydenvang, J.; Graff, T. G.; Morookian, J.-M.; Stolper, E. M.; Schwenzer, S. P. Silicic volcanism on Mars evidenced by tridymite in high-SiO2 sedimentary rock at Gale crater. *Proc. Natl. Acad. Sci. U.S.A.* **2016**, *113*, 7071−7076.

(27) Kremer, C. H.; Mustard, J. F.; Bramble, M. S. A widespread olivine-rich ash deposit on Mars. *Geology* **2019**, *47*, 677−681.

(28) Fagents, S. A.; Wilson, L. Numerical modeling of ejecta dispersal from transient volcanic explosions on Mars. *Icarus* **1996**, *123*, 284−295.

(29) Kerber, L.; Forget, F.; Madeleine, J.-B.; Wordsworth, R.; Head, J. W.; Wilson, L. The effect of atmospheric pressure on the dispersal of pyroclasts from martian volcanoes. *Icarus* **2013**, *223*, 149−156.

(30) Amador, E. S.; Cable, M. L.; Chaudry, N.; Cullen, T.; Gentry, D.; Jacobsen, M. B.; Murukesan, G.; Schwieterman, E. W.; Stevens, A. H.; Stockton, A.; Yin, C.; Cullen, D. C.; Geppert, W. Synchronous in-field application of life-detection techniques in planetary analog missions. *Planet. Space Sci.* **2015**, *106*, 1−10.

(31) Gentry, D. M.; Amador, E. S.; Cable, M. L.; Chaudry, N.; Cullen, T.; Jacobsen, M. B.; Murukesan, G.; Schwieterman, E. W.; Stevens, A. H.; Stockton, A.; Tan, G.; Yin, C.; Cullen, D. C.; Geppert, W. Correlations Between Life-Detection Techniques and Implications for Sampling Site Selection in Planetary Analog Missions. *Astrobiology* **2017**, *17*, 1009−1021.

(32) Hud, N. V. Our odyssey to find a plausible prebiotic path to RNA: the first twenty years. *Synlett* **2017**, *28*, 36−55.

(33) McKay, C. P.; Andersen, D.; Davila, A. Antarctic environments as models of planetary habitats: University Valley as a model for modern Mars and Lake Untersee as a model for Enceladus and ancient Mars. *Polar J.* **2017**, *7*, 303−318.

(34) Bertagnolli, A. D.; Padilla, C. C.; Glass, J. B.; Thamdrup, B.; Stewart, F. J. Metabolic potential and in situ activity of marine Marinimicrobia bacteria in an anoxic water column. *Environ. Microbiol.* **2017**, *19*, 4392−4416.

(35) Grotzinger, J. P.; Sumner, D. Y.; Kah, L.; Stack, K.; Gupta, S.; Edgar, L.; Rubin, D.; Lewis, K.; Schieber, J.; Mangold, N.; et al. A habitable fluvio-lacustrine environment at Yellowknife Bay, Gale Crater, Mars. *Science* **2014**, *343*, 1242777.

(36) Ehlmann, B. L.; Mustard, J. F.; Fassett, C. I.; Schon, S. C.; Head, J. W., III; Des Marais, D. J.; Grant, J. A.; Murchie, S. L. Clay minerals in delta deposits and organic preservation potential on Mars. *Nat. Geosci.* **2008**, *1*, 355−358.

(37) Goudge, T. A.; Mustard, J. F.; Head, J. W.; Fassett, C. I.; Wiseman, S. M. Assessing the mineralogy of the watershed and fan deposits of the Jezero crater paleolake system, Mars. *J. Geophys. Res.: Planets* **2015**, *120*, 775−808.

(38) Allwood, A.; Clark, B.; Flannery, D.; Hurowitz, J.; Wade, L.; Elam, T.; Foote, M.; Knowles, E. Texture-specific Elemental Analysis of Rocks and Soils with PIXL: The Planetary Instrument for X-Ray

https://dx.doi.org/10.1021/acsearthspacechem.0c00015
ACS Earth Space Chem. XXXX, XXX, XXX−XXX

Lithochemistry on Mars 2020. *2015 IEEE Aerospace Conference*; IEEE, 2015; pp 1−13.
(39) Beegle, L.; Bhartia, R.; White, M.; DeFlores, L.; Abbey, W.; Wu, Y.-H.; Cameron, B.; Moore, J.; Fries, M.; Burton, A. SHERLOC: Scanning Habitable Environments with Raman & Luminescence for Organics & Chemicals. *2015 IEEE Aerospace Conference*; IEEE, 2015; pp 1−11.
(40) Wiens, R. C.; Maurice, S.; Rull Perez, F. The SuperCam remote sensing instrument suite for the Mars 2020 rover mission: A preview. *Spectroscopy* **2017**, *32*, 50.
(41) Bennett, P. C.; Rogers, J. R.; Choi, W. J.; Hiebert, F. K. Silicates, Silicate Weathering, and Microbial Ecology. *Geomicrobiol. J.* **2001**, *18*, 3−19.
(42) Galand, P. E.; Casamayor, E. O.; Kirchman, D. L.; Lovejoy, C. Ecology of the rare microbial biosphere of the Arctic Ocean. *Proc. Natl. Acad. Sci. U.S.A.* **2009**, *106*, 22427−22432.
(43) Pedrós-Alió, C. The rare bacterial biosphere. *Annu. Rev. Mater. Sci.* **2012**, *4*, 449−466.
(44) Probandt, D.; Eickhorst, T.; Ellrott, A.; Amann, R.; Knittel, K. Microbial life on a sand grain: from bulk sediment to single grains. *ISME J.* **2018**, *12*, 623−633.
(45) Lynch, M. D. J.; Neufeld, J. D. Ecology and exploration of the rare biosphere. *Nat. Rev. Microbiol.* **2015**, *13*, 217−229.
(46) Jousset, A.; Bienhold, C.; Chatzinotas, A.; Gallien, L.; Gobet, A.; Kurm, V.; Küsel, K.; Rillig, M. C.; Rivett, D. W.; Salles, J. F.; van der Heijden, M. G. A.; Youssef, N. H.; Zhang, X.; Wei, Z.; Hol, W. H. G. Where less may be more: how the rare biosphere pulls ecosystems strings. *ISME J.* **2017**, *11*, 853−862.
(47) Shade, A.; Jones, S. E.; Caporaso, J. G.; Handelsman, J.; Knight, R.; Fierer, N.; Gilbert, J. A. Conditionally rare taxa disproportionately contribute to temporal changes in microbial diversity. *mBio* **2014**, *5*, e01371−14.
(48) Ramirez, R. M.; Craddock, R. A. The geological and climatological case for a warmer and wetter early Mars. *Nat. Geosci.* **2018**, *11*, 230−237.
(49) Hale, L.; Crowley, D. DNA extraction methodology for biochar-amended sand and clay. *Biol. Fertil. Soils* **2015**, *51*, 733−738.
(50) Love, M. I.; Huber, W.; Anders, S. Moderated estimation of fold change and dispersion for RNA-seq data with DESeq2. *Genome Biol.* **2014**, *15*, 550.
(51) Viviano-Beck, C. E.; Seelos, F. P.; Murchie, S. L.; Kahn, E. G.; Seelos, K. D.; Taylor, H. W.; Taylor, K.; Ehlmann, B. L.; Wiseman, S. M.; Mustard, J. F. Revised CRISM spectral parameters and summary products based on the currently detected mineral diversity on Mars. *J. Geophys. Res.: Planets* **2014**, *119*, 1403−1431.
(52) Pyle, D. M. The thickness, volume and grainsize of tephra fall deposits. *Bull. Volcanol.* **1989**, *51*, 1−15.
(53) Carli, C.; Serventi, G.; Sgavetti, M. VNIR spectral characteristics of terrestrial igneous effusive rocks: mineralogical composition and the influence of texture. *Geol. Soc. Spec. Publ.* **2015**, *401*, 139−158.
(54) Carli, C.; Roush, T. L.; Pedrazzi, G.; Capaccioni, F. Visible and Near-Infrared (VNIR) reflectance spectroscopy of glassy igneous material: Spectral variation, retrieving optical constants and particle sizes by Hapke model. *Icarus* **2016**, *266*, 267−278.
(55) Chini, A.; Ester Hollas, C.; Chiapetti Bolsan, A.; Venturin, B.; Bonassa, G.; Egidio Cantão, M.; Mercia Guaratini Ibelli, A.; Goldschmidt Antes, F.; Kunz, A. Process Performance and Anammox Community Diversity in a Deammonification Reactor Under Progressive Nitrogen Loading Rates for Swine Wastewater Treatment. *Bioresour. Technol.* **2020**, *311*, 123521.
(56) Fuerst, J. A.; Sagulenko, E. Beyond the bacterium: planctomycetes challenge our concepts of microbial structure and function. *Nat. Rev. Microbiol.* **2011**, *9*, 403−413.
(57) Weise, W.; Rheinheimer, G. Scanning electron microscopy and epifluorescence investigation of bacterial colonization of marine sand sediments. *Microbiol. Ecol.* **1977**, *4*, 175−188.
(58) Edwards, K. J.; Rutenberg, A. D. Microbial response to surface microtopography: the role of metabolism in localized mineral dissolution. *Chem. Geol.* **2001**, *180*, 19−32.
(59) Roberts, J. A. Inhibition and enhancement of microbial surface colonization: the role of silicate composition. *Chem. Geol.* **2004**, *212*, 313−327.
(60) Rogers, J. R.; Bennett, P. C. Mineral stimulation of subsurface microorganisms: release of limiting nutrients from silicates. *Chem. Geol.* **2004**, *203*, 91−108.
(61) Phillips-Lander, C. M.; Harrold, Z.; Hausrath, E. M.; Lanzirotti, A.; Newville, M.; Adcock, C. T.; Raymond, J. A.; Huang, S.; Tschauner, O.; Sanchez, A. Snow Algae Preferentially Grow on Fe-containing Minerals and Contribute to the Formation of Fe Phases. *Geomicrobiol. J.* **2020**, *37*, 572.
(62) Gleeson, D. B.; Kennedy, N. M.; Clipson, N.; Melville, K.; Gadd, G. M.; McDermott, F. P. Characterization of bacterial community structure on a weathered pegmatitic granite. *Microbiol. Ecol.* **2006**, *51*, 526−534.
(63) Meslier, V.; Casero, M. C.; Dailey, M.; Wierzchos, J.; Ascaso, C.; Artieda, O.; McCullough, P. R.; DiRuggiero, J. Fundamental drivers for endolithic microbial community assemblies in the hyperarid Atacama Desert. *Environ. Microbiol.* **2018**, *20*, 1765−1781.
(64) Brož, P.; Hauber, E. A unique volcanic field in Tharsis, Mars: Pyroclastic cones as evidence for explosive eruptions. *Icarus* **2012**, *218*, 88−99.
(65) Rogers, A. D.; Warner, N. H.; Golombek, M. P.; Head, J. W., III; Cowart, J. C. Areally extensive surface bedrock exposures on Mars: Many are clastic rocks, not lavas. *Geophys. Res. Lett.* **2018**, *45*, 1767−1777.
(66) La Spina, G.; Clarke, A. B.; de' Michieli Vitturi, M.; Burton, M.; Allison, C. M.; Roggensack, K.; Alfano, F. Conduit dynamics of highly explosive basaltic eruptions: The 1085 CE Sunset Crater sub-Plinian events. *J. Volcanol. Geotherm. Res.* **2019**, *387*, 106658.
(67) Crummy, J. M.; Savov, I. P.; Navarro-Ochoa, C.; Morgan, D. J.; Wilson, M. High-K Mafic Plinian Eruptions of Volcán de Colima, Mexico. *J. Petrol.* **2014**, *55*, 2155−2192.
(68) Wehrmann, H.; Bonadonna, C.; Freundt, A.; Houghton, B. F.; Kutterolf, S. Fontana Tephra: a basaltic Plinian eruption in Nicaragua. *Volcanic Hazards in Central America*; Geological Society of America, 2006; Vol. *412*, p 209.
(69) Ehlmann, B. L.; Mustard, J. F. An in-situ record of major environmental transitions on early Mars at Northeast Syrtis Major. *Geophys. Res. Lett.* **2012**, *39*, L11202.
(70) Westall, F.; Foucher, F.; Cavalazzi, B.; de Vries, S. T.; Nijman, W.; Pearson, V.; Watson, J.; Verchovsky, A.; Wright, I.; Rouzaud, J.-N.; Marchesini, D.; Anne, S. Volcaniclastic habitats for early life on Earth and Mars: A case study from ∼3.5Ga-old rocks from the Pilbara, Australia. *Planet. Space Sci.* **2011**, *59*, 1093−1106.
(71) Westall, F.; Foucher, F.; Bost, N.; Bertrand, M.; Loizeau, D.; Vago, J. L.; Kminek, G.; Gaboyer, F.; Campbell, K. A.; Bréhéret, J.-G.; Gautret, P.; Cockell, C. S. Biosignatures on Mars: What, Where, and How? Implications for the Search for Martian Life. *Astrobiology* **2015**, *15*, 998−1029.
(72) Cockell, C. S.; Balme, M.; Bridges, J. C.; Davila, A.; Schwenzer, S. P. Uninhabited habitats on Mars. *Icarus* **2012**, *217*, 184−193.
(73) De Toffoli, B.; Pozzobon, R.; Massironi, M.; Mazzarini, F.; Conway, S.; Cremonese, G. Surface expressions of subsurface sediment Mobilization Rooted into a Gas Hydrate-Rich Cryosphere on Mars. *Sci. Rep.* **2018**, *9*, 8603.
(74) Guidat, T.; Pochat, S.; Bourgeois, O.; Souček, O. Landform assemblage in Isidis Planitia, Mars: Evidence for a 3 Ga old polythermal ice sheet. *Earth Planet. Sci. Lett.* **2015**, *411*, 253−267.
(75) Hosein, R.; Haque, S.; Beckles, D. Mud volcanoes of Trinidad as astrobiological analogs for Martian environments. *Life* **2014**, *4*, 566−585.
(76) Skinner, J. A., Jr.; Mazzini, A. Martian mud volcanism: Terrestrial analogs and implications for formational scenarios. *Mar. Pet. Geol.* **2009**, *26*, 1866−1878.
(77) McKay, C. P.; Stoker, C. R.; Glass, B. J.; Davé, A. I.; Davila, A. F.; Heldmann, J. L.; Marinova, M. M.; Fairen, A. G.; Quinn, R. C.; Zacny, K. A.; Paulsen, G.; Smith, P. H.; Parro, V.; Andersen, D. T.; Hecht, M. H.; Lacelle, D.; Pollard, W. H. The Icebreaker Life Mission to Mars: a

https://dx.doi.org/10.1021/acsearthspacechem.0c00015
ACS Earth Space Chem. XXXX, XXX, XXX−XXX

search for biomolecular evidence for life. *Astrobiology* **2013**, *13*, 334−353.
(78) Costard, F.; Forget, F.; Mangold, N.; Peulvast, J. P. Formation of recent Martian debris flows by melting of near-surface ground ice at high obliquity. *Science* **2002**, *295*, 110−113.
(79) Edgar, L. A.; Gupta, S.; Rubin, D. M.; Lewis, K. W.; Kocurek, G. A.; Anderson, R. B.; Bell, J. F.; et al. Shaler: in situ analysis of a fluvial sedimentary deposit on Mars. *Sedimentology* **2013**, *65*, 96−122.
(80) McMahon, S.; Bosak, T.; Grotzinger, J. P.; Milliken, R. E.; Summons, R. E.; Daye, M.; Newman, S. A.; Fraeman, A.; Williford, K. H.; Briggs, D. E. G. A field guide to finding fossils on Mars. *J. Geophys. Res.: Planets* **2018**, *123*, 1012−1040.

https://dx.doi.org/10.1021/acsearthspacechem.0c00015
ACS Earth Space Chem. XXXX, XXX, XXX−XXX